THE JOURNAL OF BIOLOGICAL CHEMISTRY VOL. 290, NO. 46, pp. 27511–27523, November 13, 2015

Molecular Interactions and Cellular Itinerary of the Yeast RAVE (Regulator of the H^+-ATPase of Vacuolar and Endosomal Membranes) Complex*

Received for publication, May 26, 2015, and in revised form, September 9, 2015 Published, JBC Papers in Press, September 24, 2015, DOI 10.1074/jbc.M115.667634

Anne M. Smardon, Negin Dehdar Nasab, Maureen Tarsio, Theodore T. Diakov, and Patricia M. Kane[1]

From the Department of Biochemistry and Molecular Biology, SUNY Upstate Medical University, Syracuse, New York 13210

Background: The RAVE complex is required for glucose-sensitive V-ATPase assembly, but its mechanism is unknown.
Results: Newly defined RAVE-V-ATPase interactions suggest assembly mechanisms.
Conclusion: RAVE shows glucose-sensitive interactions with vacuolar membranes and may help orient V-ATPase subunit C during assembly.
Significance: Mammalian rabconnectins likely require similar V-ATPase interactions to support V-ATPase assembly and may be reversibly recruited to membranes.

The RAVE complex (regulator of the H^+-ATPase of vacuolar and endosomal membranes) is required for biosynthetic assembly and glucose-stimulated reassembly of the yeast vacuolar H^+-ATPase (V-ATPase). Yeast RAVE contains three subunits: Rav1, Rav2, and Skp1. Rav1 is the largest subunit, and it binds Rav2 and Skp1 of RAVE; the E, G, and C subunits of the V-ATPase peripheral V_1 sector; and Vph1 of the membrane V_o sector. We identified Rav1 regions required for interaction with its binding partners through deletion analysis, co-immunoprecipitation, two-hybrid assay, and pulldown assays with expressed proteins. We find that Skp1 binding requires sequences near the C terminus of Rav1, V_1 subunits E and C bind to a conserved region in the C-terminal half of Rav1, and the cytosolic domain of Vph1 binds near the junction of the Rav1 N- and C-terminal halves. In contrast, Rav2 binds to the N-terminal domain of Rav1, which can be modeled as a double β-propeller. Only the V_1 C subunit binds to both Rav1 and Rav2. Using GFP-tagged RAVE subunits *in vivo*, we demonstrate glucose-dependent association of RAVE with the vacuolar membrane, consistent with its role in glucose-dependent V-ATPase assembly. It is known that V_1 subunit C localizes to the V_1-V_o interface in assembled V-ATPase complexes and is important in regulated disassembly of V-ATPases. We propose that RAVE cycles between cytosol and vacuolar membrane in a glucose-dependent manner, positioning V_1 and V_0 subcomplexes and orienting the V_1 C subunit to promote assembly.

Vacuolar H^+-ATPases (V-ATPases)[2] are ubiquitous and highly conserved proton pumps found in all eukaryotic cells (1, 2). The V-ATPase is a multisubunit enzyme comprised of a peripheral complex containing sites of ATP hydrolysis, called V_1, and an integral membrane complex containing the proton pore, called V_o. The V_1 complex contains eight subunits designated A to H, and the V_o complex contains six subunits designated a, c, c′, c″, d, and e. In yeast, the V-ATPase subunits are encoded by single-copy *VMA* genes, with the exception of the V_o a subunit, which has two isoforms encoded by the *VPH1* and *STV1* genes (1). ATP-driven proton transport requires stable association of the V_1 and V_o complexes; free V_1 is inactive as a Mg^{2+}-dependent ATPase, and free V_o sectors are closed to H^+ transport (3–5). Inactivation of the disassembled sectors is physiologically significant, because V-ATPases are regulated by a reversible disassembly mechanism through which V_1 sectors are partially detached from V_o in response to glucose deprivation and reassembled upon glucose readdition (6–8).

The yeast RAVE (regulator of the H^+-ATPase of vacuoles and endosomes) complex is required for both the initial biosynthetic assembly of the V-ATPase and for reassembly of the complex after glucose deprivation and readdition (9, 10). RAVE contains three subunits: Rav1, Rav2, and Skp1 (9). Initial experiments established that Rav2 and Skp1 bind to Rav1, but not to each other, and that RAVE exists as a stable complex with Rav1 as the central component (9, 10). Skp1 participates in multiple cellular complexes, including the SCF (Skp1-cullin-F-box) ubiquitin ligases, and loss of *SKP1* is lethal (11, 12). In contrast, *rav1*Δ and *rav2*Δ mutants exhibit a Vma^- growth phenotype, characterized by poor growth at high pH and/or elevated calcium concentrations, but unlike other *vma* mutants only display this phenotype at elevated temperature (13).

Although the composition of the RAVE complex is quite well established, neither the basis of its activity in promoting V-ATPase assembly nor the sites of interaction between Rav1 and its partners are understood. Under conditions of V-ATPase disassembly, RAVE binds to V_1 sectors in cytosolic fractions via the E and/or G subunits of V_1, but this interaction is not intrinsically glucose-sensitive (10, 11). Rav1 also has a binding site for the cytosolic N-terminal domain of V_o subunit Vph1 (13). The V_1 C subunit is present at the interface of the V_1 and V_o sectors and is thus positioned to play a critical role in reversible disas-

* This work was supported by National Institutes of Health Grants R01 GM50322 and R01 GM63742 (to P. M. K.) and an American Heart Association postdoctoral fellowship (to A. M. S.). The authors declare that they have no conflicts of interest with the contents of this article.
[1] To whom correspondence should be addressed: Dept. of Biochemistry and Molecular Biology, SUNY Upstate Medical University, 750 East Adams St., Syracuse, NY 13210. Tel.: 315-464-8742; Fax: 315-464-8750; E-mail: kanepm@upstate.edu.
[2] The abbreviation used is: V-ATPase, vacuolar H^+-ATPase.

TABLE 1
Yeast strains used in this study

Strain	Genotype	Source
SF838-5A RAV1-Myc13	*MATα ura3-52 leu2-3,112 his4-519 ade6* RAV1-Myc13-kanMX6	Ref. 10
SF838-5A *rav1-Δ840-Myc13*	*MATα ura3-52 leu2-3,112 his4-519 ade6 rav1-Δ840-Myc13-kanMX6*	This study
SF838-5A *rav1-Δ941-Myc13*	*MATα ura3-52 leu2-3,112 his4-519 ade6 rav1-Δ941-Myc13-kanMX6*	This study
SF838-5A *rav1-Δ1126-Myc13*	*MATα ura3-52 leu2-3,112 his4-519 ade6 rav1-Δ1126-Myc13-kanMX6*	This study
SF838-5A *rav1-Δ1271-Myc13*	*MATα ura3-52 leu2-3,112 his4-519 ade6 rav1-Δ1271-Myc13-kanMX6*	This study
SF838-5A *vma5Δ*	*MATα ura3-52 leu2-3,112 his4-519 ade6 vma5Δ::kanMX6*	This study
SF838-5A RAV2-Myc13	*MATα ura3-52 leu2-3,112 his4-519 ade6 RAV2-Myc13-kanMX6*	This study
SF838-5A RAV2-Myc13 *vma5Δ*	*MATα ura3-52 leu2-3,112 his4-519 ade6 RAV2-Myc13-kanMX6 vma5Δ::kanMX6*	This study
SF838-5A *FLAG-VMA5*	*MATα ura3-52 leu2-3,112 his4-519 ade6* FLAG-VMA5	This study
SF838-5A *RAV2-Myc13 FLAG-VMA5*	*MATα ura3-52 leu2-3,112 his4-519 ade6 RAV2-Myc13-kanMX6 FLAG-VMA5*	This study
SF838-5A *RAV2-Myc13 FLAG-VMA5 rav1Δ*	*MATα ura3-52 leu2-3,112 his4-519 ade6 RAV2-Myc13-kanMX6 FLAG-VMA5 rav1Δ::LEU2*	This study
SF838-5A RAV1-GFP	*MATα ura3-52 leu2-3,112 his4-519 ade6 RAV1-GFP-kanMX6*	This study
SF838-5A RAV2-GFP	*MATα ura3-52 leu2-3,112 his4-519 ade6 RAV2-GFP-kanMX6*	This study
PJ69-4A	*MATa trp1-901 leu2-3,112 ura3-52 his3-200 gal4Δ gal80Δ LYS2::GAL1-HIS3 GAL2-ADE2 met2::GAL7-lacZ*	Ref. 35
PJ69-4α	*MATα trp1-901 leu2-3,112 ura3-52 his3-200 gal4Δ gal80Δ LYS2::GAL1-HIS3 GAL2-ADE2 met2::GAL7-lacZ*	Ref. 35

sembly of the V-ATPase (14–16). Interestingly, this subunit is released from both the V_1 and V_o sectors when the V-ATPase disassembles (6, 17). Subunit C binds to Rav1 independently of the V_1 subcomplex and is the only subunit that has shown any binding to Rav2 (18). Binding of RAVE to detached V_1 sectors, V_1 subunit C, and V_o subunit Vph1 is intriguing, because it suggests that RAVE might act by bringing these subunits together to establish or re-establish V_1-V_o assembly. However, without any information about structure or binding sites on RAVE, this proposed activity remains speculative.

RAVE function in V-ATPase assembly appears to be conserved in higher eukaryotes. Higher eukaryotes contain larger rabconnectin-3 complexes consisting of two subunits, rabconnectin-3α (also called DMXL2 in humans) and rabconnectin-3β (also called WDR7 in humans) (19). Mutations in either subunit have been shown to result in organelle acidification defects (20–22), and in zebrafish hair cells, lower levels of V_1-V_o association were observed in a rabconnectin loss of function mutant (22). V-ATPase subunits co-immunoprecipitate with DMXL2 (23). Although other fungi contain *RAV2* homologues, there is no sequence homology between the rabconnectin subunits and *RAV2*. In contrast, a highly conserved region has been identified in fungal *RAV1* homologues and in mammalian rabconnectin-3α subunits and designated the "Rav1-C superfamily" (24). This region extends from amino acids 571 to 1191 of yeast *RAV1*, but the *RAV1* sequence between amino acids 840 and 1125 is the most highly conserved across all species (25). In addition, the N-terminal 240 amino acids of yeast RAV1 also align with the N termini of rabconnectin-3α homologues of higher organisms. Based on sequence comparisons with both other fungi and higher eukaryotes, we identified six regions of Rav1 that are conserved to differing degrees (25).

Many questions remain about RAVE/rabconnectin structure and function. Although multiple interactions between the V-ATPase and yeast RAVE have been identified, these interactions have not been mapped to specific regions of the RAVE complex. Mapping these interactions could provide insights into the mechanism of RAVE-promoted assembly. In addition, although RAVE participates in glucose-sensitive reversible disassembly of the V-ATPase, it has not been determined which interactions with RAVE might be glucose-sensitive. Given the high level of sequence conservation among all eukaryotic V-ATPases and the evidence that RAVE and rabconnectin complexes both regulate V-ATPase activity at the level of V_1-V_o assembly, we hypothesized that functionally critical V-ATPase subunit binding sites might be located in the conserved regions of Rav1. In this work, we test this hypothesis by generating a series of deletions and fragments of Rav1 and evaluating their binding to V-ATPase subunit partners. In addition, we demonstrate that the RAVE complex shows glucose-dependent association with the vacuolar membrane *in vivo*, consistent with its role in glucose-dependent V-ATPase assembly.

Experimental Procedures

Materials and Growth Media—Oligonucleotides were purchased from MWG Operon. Anti-FLAG-M2 resin, mouse anti-FLAG-M2 antibody, and FLAG peptide were purchased from Sigma. Amylose resin was purchased from New England Biolabs, and glutathione-Sepharose was from GenScript. TALON resin, for purification of His_6-tagged protein, was obtained from Clontech. Anti-myc monoclonal antibody (9E10) was purchased from Roche Applied Science. Media for growth of yeast and *Escherichia coli* were from Fisher Scientific.

Yeast cells were maintained in rich medium, YEPD (yeast extract, peptone, 2% dextrose) medium buffered to pH 5 with 50 mM potassium phosphate and 50 mM potassium succinate, or in fully supplemented minimal medium (SC) with individual nutrients omitted for selection as indicated. The Vma^- phenotype was tested by comparing growth of cells on YEPD plates buffered to pH 5 to growth on YEPD plates buffered to pH 7.5 with 50 mM MES and 50 mM MOPS, to which 60 mM $CaCl_2$ was added.

Yeast Strain Construction—The yeast strains used in this work are listed in Table 1. Strains containing integrated C-terminal deletions of *RAV1* followed by an in frame myc_{13} tag were constructed using fusion PCR as previously described (10). Briefly the myc_{13}-kanMX cassette from the plasmid pFA6a-myc_{13}-kanMX (26) was amplified. This was followed by amplification of *RAV1* fragments immediately upstream of each desired terminal amino acid (at positions 839, 939, 1125, and 1270) using the following oligonucleotide pairs, respectively: R1M6-5p and RAV1M6; R1M7-5p and RAV1M7; R1M5-5p and RAV1M5; and R1M5-5p and RAV1M13. (Oligonucleotide sequences are shown in Table 2.) Another *RAV1* PCR fragment immediately downstream of the stop codon was amplified using oligonucleotides RAV1M3 and YJR9. The final myc_{13}-tagged, C-terminally deleted *RAV1* fusion products were generated for each deletion as previously described (27). The wild type strain

TABLE 2
Oligonucleotides used in this study

Oligonucleotide name	Oligonucleotide sequence (5′-3′)
RAV1M2	TCACCGTTAATTAACCCGGGGATCCGTACAAAGTCATCTAGTAAGTTCTTGGTAATAGC
RAV1M3	CATCCAGTTTAAACGAGCTCGAATTCCAGCCTTACAAGTAACTAATTAGGAG[i]
RAV1M5	TCACCGTTAATTAACCCGGGGATCCGAACAATGCTTGAGTTGTTTTCTAAATCAATCGG
RAV1M6	TCACCGTTAATTAACCCGGGGATCCGTGCTAGAGACACTGTCTTATTGAAACAG
RAV1M7	TCACCGTTAATTAACCCGGGGATCCGATAGGCTATTCTATATTCTCGAGCGCGATT
RAV1M13	GTTAATTAACCCGGGGATCCGTGGTGGTTGCAAGAAGTCGTCTAAT
R1M5-5p	GTGTCAACGTTCTTTGCAAGCAAGTGC
R1M6-5p	TGGTCCACTTCCAGTTTATCATCCAC
R1M7-5p	GACAGTGTCTCTAGCACTTACTGAG
RAV1BamHI	GCGGATCCTCATGTCATTGAACTTTCTTCCAGGACG
RAV1-NT2H-3	AGGTCGACCACAGTATGGTTTTTCTCCATTTC
RAV1-2H-679	GCCATGGAGGCCCCGGGGAACACACCTAGTTACCTACCTATTG
RAV1-2H-840	CTTGGCTGCAGGTCGACAAGTGCTAGAGACACTGTCTTATTG
RAV1-CT2H-5	GGCCAGATCTCTTACTGAGCAACTAACGAAAACAAC
RAV1-CT2H-3	AGGTCGACAACAATGCTTGAGTTGTTTTCTAAATC
RAV1M8-2Hyb2	CTCCCGGGAATGCAAATATGGGGTGAAGTGCC
RAV1M9-2Hyb	CTCCCGGGATCATTGAACTTTCTTCCAGGACGCC
R1-M11F	CTTACCAGAACGTATAAAGCCATCCTTACTGAGCAACTAACGAAAACAAC
R1-M11R	GTTGTTTTCGTTAGTTGCTCAGTAAGGATGGCTTTATACGTTCTGGTAAG
R1-M14F	TTCAATAAGACAGTGTCTCTAGCAGATAAGGAAGTCTGTGTTAACAGA
R1-M14R	TCTGTTAACACAGACTTCCTTATCTGCTAGAGACACTGTCTTATTGAA
YJR7	CCATCTCCTCCCTCGGATCAAACTTTC
YJR9	ATACATGCCTGAACCCGACGTAGACA
YJR10	TTTCACCCACAGAGTCGTTTCGGCATCAGAGCAGATTGTA
YJR11	GCCTTGATCCATTGGACATGCCTATC
RAV2M1	CGGTGTACAAGTCCAGGATTCCAC
RAV2M2	TCACCGTTAATTAACCCGGGGATCCGCTTATATGTACTTAACTGTTTGCTAGCTAC
RAV2M3	CATCCAGTTTAAACGAGCTCGAATTCCCAACTTATTCTCCAGTTGCTTCTTC
YDR6-6	CCGTTTAGTTCCCGAATATG
VMA5-600	TTGTTGACGGTAAGGTTTTGAAATAATCTC
VMA5 + 350	GGTTTAAAGTCGACCTGTAGTGC
FL1-5	CATCGTCGTCCTTGTAGTCCATTTTTTTTTTTCAGAAAAAAGAATTG
FL2-5	GACTACAAGGACGACGATGACAAGGCTACTGCGTTATATACTGCAAAC
rav1679-R1	CGCGAATTCAACACACCTAGTTACCTACCTATTG
rav1898-Sal1	GCGGTCGACTTATTGAATATTTTTATGTGATAAAAATAACTTCAC
Rav(679–898)-HisF	CAACACCACCATCATCACCACTAAGTCGACCTGCAGGCAAGCTTGG
Rav(679–898)-HisR	TTAGTGGTGATGATGGTGGTGTTGAATATTTTTATGTGATAAAAATAACTTCACGC
Rav1NTerm BamHI	GCGGATCCTCATTGAACTTTCTTCCAGGAC
Rav1 NTerm SalI	GCGTCGACTTAGTGGTGATGGTGATGATGATCAGTCAAATCCAGAGATTTATC
Rav2 BamHI frw	GCGGATCCATGAGTGTTGATTTGTTTCCAAATG
Rav2 Sal1 rvs	GCGTCGACTTACTTATCGTCGTCATCCTTGTAATCCTTATATGTACTTAACTGTTTGCTA

SF838-5Aα was transformed with each fusion product using a lithium acetate method (28), and transformants were selected on YEPD medium containing 200 μg/ml G418 and confirmed by DNA sequencing and immunoblotting.

A single FLAG tag was fused to the N terminus of Vma5 to generate the yeast FLAG-*VMA5* strains. A fusion PCR protocol was used in which two individual PCR products were produced using oligonucleotide pairs VMA5-600/F1-5 and F1-2/VMA5 + 350 with genomic DNA as a template, followed by a fusion PCR using oligonucleotides VMA5-600/VMA5 + 350. The resulting fusion PCR product was used to transform an SF838-5Aα *vma5*Δ::*kanMX* strain and colonies able to grow on YEPD pH 7.5 plates were selected. Integration of the FLAG-*VMA5* was confirmed by DNA sequencing and expression of the tagged protein by immunoblotting. The *RAV2*-myc$_{13}$ strains were also constructed as described above, by fusing the myc$_{13}$*kanMX* cassette to *RAV2* fragments upstream and downstream of the stop codon, generated by PCR using oligonucleotides RAV2M1 and RAV2M2 and oligonucleotides RAV2M3 and YDR6-6, respectively. The final myc$_{13}$-tagged *RAV2* was transformed into the SF838-5Aα *vma5*Δ strain and SF838-5Aα FLAG-*VMA5* strain as described above. *RAV1* was deleted in the *RAV2*-myc$_{13}$ FLAG-*VMA5* by amplifying the *rav1*Δ::*LEU2* allele from a SF838-5Aα *rav1*Δ::*LEU2* strain using oligonucleotides YJR7 and YJR9 and transforming the PCR product into *RAV2*-myc$_{13}$ FLAG-*VMA5*. The deletion was confirmed by PCR and testing for the *rav1*Δ phenotype. The *RAV1*-GFP and *RAV2*-GFP strains were constructed using the plasmid pFA6a-GFP-*kanMX* as described previously (27, 29). The *vma5*Δ allele was introduced into the *RAV1*-GFP and *RAV2*-GFP strains by amplifying the deletion allele from a *vma5*Δ::*LEU2* strain (30) and transforming the GFP-tagged RAVE strains with this allele.

Bacterial Expression Constructs and Protein Purification—The MBP (maltose-binding protein)-Rav1NT-His$_6$ expression plasmid was constructed by amplifying the sequence corresponding to amino acids 2–729 of *RAV1* by PCR using oligonucleotides Rav1 NTerm BamHI and Rav1 NTerm SalI (which introduces the His$_6$ tag just before the stop codon) and a combination of LA-*Taq* (TaKaRa) and *Pfu* (New England Biolabs) polymerases to enhance fidelity. The resulting PCR fragment was cloned into the pGEM T-Easy vector (Promega) after A-tailing with *Taq* polymerase (Fisher). The insert was verified by sequencing at the Upstate DNA sequencing facility. Digestion with BamHI and SalI removed the insert, which was ligated to the pMAL-pAse vector (31) that had been digested with BamHI and SalI. The MBP-*RAV2*-FLAG construct was constructed by PCR amplifying the entire *RAV2* sequence using oligonucleotides Rav2BamHI forward and Rav2SalI reverse (which introduces a single FLAG tag immediately before the stop codon). The amplified fragment was cloned into the

pGEM T-Easy and pMAL-pAse vectors as described above. The MBP-*RAV1*(679–898)-His_6 expression plasmid was constructed in two steps. First, the *RAV1* fragment corresponding to amino acids 679–898 was amplified by PCR, using oligonucleotides (Rav1679RI and Rav1898-SalI), and this fragment was cloned into the pMAL-pAse vector as described above. The His_6 tag was subsequently added by inverse PCR mutagenesis using oligonucleotides (Rav(679–898)-HisF and Rav(679–898)-HisR) to generate a mutagenized PCR product, followed by digestion of the unmutagenized template with DpnI and transformation of *E. coli* DH5α cells. Incorporation of the tag was confirmed by sequencing. Construction of GST-tagged Rav1(840–1125) (13), MBP-Vph1NT (31), and MBP-V_1C (15) expression vectors have been described.

All of the above expression plasmids were introduced into *E. coli* expression strain BL21, with the exception of MBP-V_1C, which was expressed in the Rosetta2 strain. Cells containing the expression plasmids were grown in rich broth (Luria broth supplemented with 2% glucose and 125 mg/ml ampicillin) to a density of 0.5–0.6 A_{600}/ml, and then 0.5 mM isopropyl β-D-thiogalactopyranoside was added to induce expression. Induction conditions were as follows: 6 h at 30 °C for MBP-Rav1NT-His_6, 2 h at 37 °C for MBP-Rav2-FLAG and MBP-Rav1(679–898)-His6, and 16 h at 19 °C for MBP-Vph1NT(1–372). After inductions, cell pellets were frozen at −80 °C and then lysed by sonication after addition of 50 ml of amylose column buffer (20 mM Tris-HCl, 200 mM NaCl, 1 mM EDTA, pH 7.2) per liter of cell pellet. PMSF and β-mercaptoethanol were added to 1 and 5 mM, respectively, immediately before lysis. The MBP-tagged proteins were then affinity-purified by binding to amylose columns, washing with 12 column volumes of amylose column buffer, and elution with 10 mM maltose in column buffer. In experiments where MBP was removed, the peak fractions containing MBP fusion protein were combined and incubated with 10 μg of Prescission protease overnight at 4 °C. FLAG-tagged proteins were further purified on a anti-FLAG-M2 affinity column using FLAG column buffer (20 mM Tris-HCl, 150 mM NaCl, 1 mM EDTA, pH 7.2) for loading and washes. Tagged protein was eluted in the same buffer containing 100 μg/ml FLAG peptide. For purification on TALON resin, His_6-tagged proteins were dialyzed into 50 mM sodium phosphate, pH 7.5, 150 mM NaCl containing 5 mM β-mercaptoethanol. The His_6-tagged protein was mixed with 0.5 ml of TALON resin, either in the presence or absence of its interacting partner, and incubated with mixing for 1 h. at 4 °C. The resin was then poured into a column for washing with the same buffer containing 5 mM imidazole, followed by elution with 50 mM phosphate, pH 7.5, 300 mM NaCl, and 250 mM imidazole. 0.5-ml fractions were collected during the elution, and peak fractions, based on absorbance at 280 nm, were combined and precipitated with 10% trichloroacetic acid. Purification of GST-Rav1(840–1125) was described previously (13).

All of the expressed protein-protein interactions were observed at least three times, except the Rav1NT-Rav2 interaction experiment, which was done twice. The gels and immunoblots in Figs. 3–5 show representative experiments.

Immunoprecipitations and Immunoblots—For co-immunoprecipitations of myc-tagged Rav1 deletions with V_1B and Skp1, yeast cytosolic fractions were prepared from each *rav1* deletion strain as previously described (18). Protein concentrations of the cytosolic fractions were measured by Lowry assay (32); 0.4 mg of protein was precipitated with trichloroacetic acid (input), and 4.0 mg of cytosol were combined with 100 μl of anti-V_1B monoclonal antibody (13D11) or 6 μl of anti-myc monoclonal antibody (9E10) followed by the addition of 60 μl of a 50% (v/v) suspension of protein A-Sepharose CL4B (Sigma). The input and immunoprecipitates were solubilized at 75 °C in cracking buffer (50 mM Tris-Cl, pH 6.8, 8 M urea, 5% SDS, 5% β-mercaptoethanol) for analysis on SDS-PAGE. Western blots were probed with mouse monoclonals 9E10 (anti-myc) or 13D11 (anti-yeast Vma2 (33)) or with rabbit polyclonal anti-Skp1 antibody (a generous gift from Ray Deshaies (Caltech)).

For co-immunoprecipitation of FLAG-V_1C with Rav2-myc_{13}, whole cell lysates were prepared as previously described (10). Briefly cells (30 A_{600} of each strain) were resuspended in TBS buffer (50 mM Tris-HCl, 150 mM NaCl, pH 7.4) and lysed by agitation with glass beads. Lysates were incubated with 20 μl of anti-FLAG M2 resin at 4 °C and washed with TBS. The FLAG-V_1C fusion protein was eluted with 100 μg/ml FLAG peptide in TBS. Eluted proteins were analyzed on SDS-PAGE, and Western blots were probed with anti-myc and anti-FLAG antibodies.

Two-hybrid Analysis—The two-hybrid plasmids pAS-*RAV1*, pACT-*RAV2*, pACT-*VMA4*, and pACT-*VMA5* and the plasmid pACT-*VPH1*-NT containing the first 406 N-terminal amino acids of *VPH1* have been described previously (18, 31). pAS2 plasmids (34) containing *RAV1* fragments were constructed as follows. A *RAV1* fragment encoding amino acids 2–240 was amplified from yeast genomic DNA using oligonucleotides RAV1BamHI and RAV1-NT2H-3. The PCR product was then cloned into the pGEM-T Easy and sequenced as described above. The 716-bp BamHI/SalI fragment was excised and cloned into the pAS2 vector. Rav1 fragments containing amino acids 679–840 and 840–1125 were cloned into the pAS2 vector in a similar manner after PCR amplification with oligonucleotide pairs RAV1-2H-679 and RAV1-2H-840 and oligonucleotide pairs RAV1-CT2H-5 and RAV1-CT2H-3, respectively. Both PCR products were cloned into the pGEM-T Easy vector and then into the pAS2 vector as described above.

The pAS2 plasmids containing the *RAV1* C-terminal deletion mutants, Δ840-stop and Δ940-stop were constructed as follows. Yeast strains containing the corresponding C-terminal deletions in Rav1 described above were used as templates and the oligonucleotide pairs YJR10 and RAV1M6 for Δ840-stop and YJR10 and RAV1M7 for Δ940-stop. The PCR products generated were then cloned in the pGEM-T Easy cloning vector that was then cleaved with EcoRI-SmaI to release the inserted C-terminal *RAV1* fragments. The Rav1 fragments containing the C-terminal *RAV1* deletions were cloned into the pAS-*RAV1* plasmid and sequenced for accuracy. For internal *RAV1* deletions Δ840–1125 and Δ580–839, the following method was used. A *RAV1* PCR fragment was generated using wild type genomic DNA as template and the oligonucleotide pair YJR10 and RAV1M2. The Δ840–1125 mutation was introduced using the pAltered Sites protocol (Promega) and oligonucleotides R1M14F and R1M14R. The deletion mutation was sequenced

for accuracy, and the mutant *RAV1* was cloned into the pAS-*RAV1* plasmid that had been cleaved with Cla1-Sal1 to remove the unmutagenized Cla1-Sal1 fragment. The Δ580–839 was constructed in a similar manner using oligonucleotides R1M11F and R1M11R. The pAS2 plasmids containing the N-terminal deletions Δ2–240 and Δ98–240 were constructed by amplifying the desired fragments by PCR using the original pAS-*RAV1* plasmid as template and the oligonucleotides RAV1M8-2Hyb2 and YJR11 for Δ2–240 and RAV1M9-2Hyb and YJR11 for Δ98–240. The resulting PCR products were cloned into the pGEM-T Easy vector, sequenced for accuracy and subsequently excised with Sma1 and Cla1. The Sma1-Cla1 fragment containing the Δ2–240 and the Δ98–240 mutations were cloned into the pAS-*RAV1* plasmid that had been cleaved with Sma1-Cla1 to remove the original RAV1 N-terminal full-length fragment.

pAS and pACT plasmid constructs were transformed into the two-hybrid reporter strains PJ69-4A (*MAT**a***) and PJ69-4α (*MAT*α), respectively. *MAT**a*** strains containing pAS plasmids were crossed to *MAT*α strains containing pACT plasmids, and diploids were selected by growth on SC medium lacking leucine and tryptophan. The resulting diploids were tested for expression of two-hybrid reporter genes by plating onto plates lacking adenine and histidine, as well as leucine and tryptophan (35).

Fluorescence Microscopy—Yeast strains expressing Rav1-GFP and Rav2-GFP were grown to log phase in SC medium and visualized directly using a Zeiss Imager.Z1 fluorescence microscope equipped with a Hamamatsu CCD camera and AxioVision software. Micrographs were assembled into figures using Adobe Photoshop CS4.

Results

Rav1 Is Predicted to Have Structurally Distinct N- and C-terminal Halves—There are no three-dimensional structures for Rav1, Rav2, or either of the rabconnectin subunits, although we did previously identify six regions of Rav1 with varied levels of sequence conservation (Fig. 1*A* (25)). Secondary structure prediction (Psipred (36)) indicates that the N-terminal 720 amino acids of Rav1 have a very high content of β-sheet, amino acids 746–1194 have a high helical content, and the C-terminal 153 amino acids are likely to be very disordered (Fig. 1*A*). The amino acids between the β-sheet and α-helix rich regions (amino acids 721–745) are predominantly disordered, suggesting that the two halves of Rav1 might behave somewhat independently, with the most highly conserved Rav1-C superfamily sequences mapping predominantly to the C-terminal half rich in α-helices, and the conserved N terminus mapping to the region rich in β-sheet. We combined the information from sequence comparisons and secondary structure prediction of Rav1 to design deletion mutations and fragments that could be tested for interactions with Rav2, Skp1, and V-ATPase subunits.

The C-terminal Half of Rav1 Is Required for Efficient Binding to V_1 and Skp1—To begin to address the distribution of binding sites in the C-terminal half of Rav1, we used information from sequence comparisons to design myc-tagged C-terminal deletions through the most highly conserved region of yeast *RAV1* and then inserted them at the *RAV1* locus (Fig. 1*A*). Fig. 1*B* demonstrates that the shortest deletion, which removed only the very poorly conserved last 86 amino acids of Rav1, supported wild type growth on YEPD, pH 7.5 plates containing 60 mM $CaCl_2$ at 37 °C, suggesting that the RAVE complex is functional. In contrast, all of the other truncations resulted in a *rav1*Δ phenotype, characterized by growth on YEPD plates buffered to pH 5 but not on YEPD, pH 7.5 plates with added $CaCl_2$, indicating that they impact RAVE function. The truncations produced stable mutant Rav1 proteins, as shown by Western blotting with anti-myc antibodies (Fig. 1*C*). We immuno-

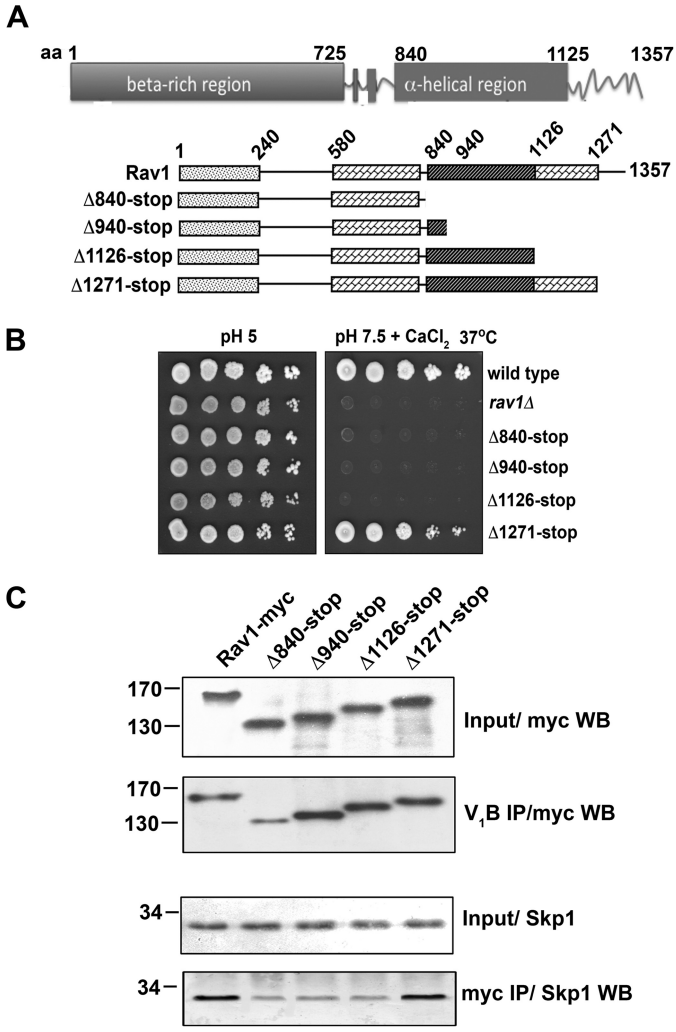

FIGURE 1. **The C-terminal half of Rav1 is required for efficient binding of V_1 and Skp1.** *A*, secondary structure of Rav1 was determined using PsiPred, and regions rich in β-sheet and α-helices are shown. Six regions of Rav1 previously determined to show varied levels of homology are indicated (25), and deletions were designed in part based on the regions of differential homology. Deletions were integrated at the *RAV1* genomic locus, and wild type and mutant proteins were tagged with the myc_{13} epitope at their C termini as described under "Experimental Procedures." *B*, strains were tested for a *rav1*Δ phenotype by growing strains to log phase in YEPD pH 5, diluting to an A_{600} of 0.5 and serially diluting 10-fold in a microtiter plate. Cells were transferred to YEPD, pH 5 plates and grown for 3 days at 37 °C and YEPD, pH 7.5 + 60 mM $CaCl_2$ plates and grown for 5 days at 37 °C. *C*, cytosolic fractions were prepared from each strain, and 0.4 mg of cytosol from each strain was directly trichloroacetic acid-precipitated and run as *Input*. Cytosolic proteins (4 mg) from each strain were immunoprecipitated separately with an antibody against V_1 subunit B (13D11) or a monoclonal antibody against the myc epitope (9E10). Immunoprecipitations were separated by SDS-PAGE and immunoblotted with anti-myc or polyclonal Skp1 antibody. The experiment shown is representative of three independent experiments. *WB*, Western blot.

precipitated myc-tagged wild type and mutant Rav1 and assessed co-precipitation of Skp1 by immunoblotting. Similar levels of Skp1 were co-precipitated with full-length Rav1-myc$_{13}$ and the shortest truncation (Δ1126-stop), but all of the other truncations immunoprecipitated much less Skp1. In contrast, anti-V_1B subunit antibodies co-precipitate the Rav1-myc$_{13}$ constructs Δ1126-stop and Δ941-stop mutations, as well as wild type Rav1-myc$_{13}$. Only in the Rav1Δ841-stop did the V_1 interaction with Rav1 appear to be decreased. Although these data cannot prove direct binding between a deleted region and V_1 or Skp1, they do indicate a requirement for amino acids 1126–1271 for Skp1 binding and amino acids 840–941 for V_1 binding. In addition, they indicate that the final 86 amino acids of Rav1 are dispensable for RAVE function.

We previously identified a number of two-hybrid interactions of intact Rav1 with Rav2; V_1 subunits E, G, and C; and the N-terminal domain of V_o subunit a isoform Vph1 (13, 18). To identify regions of the Rav1 protein required for these interactions, we expressed fragments of Rav1 that contained fragments of the C-terminal conserved domain or deletions in this domain and then tested for interactions with the Rav1-binding partners in the two-hybrid assay (Fig. 2). In this version of the two-hybrid assay, interacting partners promote transcription of the *ADE2* and *HIS3* genes and enable diploid cells containing those partners to grow in medium lacking adenine and histidine. The Rav1 fragments were tested, and their interactions with Vma4 (V_1E), Vma5 (V_1C), Rav2, and Vph1NT (the N-terminal cytosolic domain of the Vph1 isoform of V_o subunit a) are scored on the *top* of Fig. 2, and growth of the diploids on plates lacking adenine and histidine is shown at the *bottom* of Fig. 2. Consistent with immunoprecipitation results described above, the Rav1(840–1125) fragment exhibited a strong two-hybrid interaction with V_1E, one of the V-ATPase subunits shown to support the interaction of RAVE with the V_1 complex (10). No interactions with V_1E were observed with the other two small fragments tested. We complemented the two-hybrid interactions with Rav1 fragments by testing two-hybrid interactions between Rav1 deletions and V_1E. These interactions can be more complex but were consistent with the fragment interactions overall. A Rav1 deletion allele terminating at amino acid 840, as well as a deletion allele removing the highly conserved segment between amino acids 840–1125, decreased the two-hybrid interaction with V_1E. However, the interaction with V_1E remained strong in the deletion terminating at amino acid 940 and in a deletion removing amino acids 890–940. This set of interactions highlights the importance of Rav1 amino acids 840–890 for the Rav1-V_1E interaction and also implicates this region in RAVE-V_1 binding, previously shown to depend on V_1 subunits E and G (10).

Binding of Rav2 to the N-terminal Conserved Domain of Rav1—The N-terminal 240 amino acids of Rav1 constitute the second most highly conserved region among Rav1 homologues (25). When this region was expressed separately in the two-hybrid vector, it showed no interaction with V_1E but did exhibit a two-hybrid interaction with V_1C, Vph1NT, and Rav2 (Fig. 2). Deletion of the N-terminal 240 amino acids of the full Rav1 compromised the two-hybrid interactions of V_1C, Vph1NT, and Rav2, as expected by the interaction of these proteins with the Rav1 N-terminal fragment. However, deletion of only amino acids 98–240 of Rav1 largely restored the two-hybrid interaction with Rav2. These results suggest that Rav2 requires the first 98 amino acids for binding to Rav1.

We confirmed the interaction of Rav2 in the first half of Rav1 through expression of these two proteins in *E. coli* and testing for interaction *in vitro*. The first 729 amino acids of Rav1 were expressed with an N-terminal MBP tag and a C-terminal His$_6$ tag, and the full-length Rav2 was expressed with an N-terminal MBP and a C-terminal FLAG tag. Both proteins were purified via the MBP tag on amylose columns, and the MBP tag was cleaved from MBP-Rav2-FLAG (Fig. 3). When Rav2-FLAG was applied to the anti-FLAG affinity column, it eluted as a single band of the expected molecular mass (Fig. 3*A*). MBP-Rav1NT-His$_6$ did not bind to the FLAG resin without bound Rav2-FLAG (Fig. 3*B*). However, when MBP-Rav1-His$_6$, which had been further affinity-purified via the His$_6$ tag, was added to the anti-FLAG affinity column to which Rav2-FLAG had been bound, it co-eluted with Rav2 (Fig. 3*C*). These data confirm that Rav2 can bind to the N-terminal region of Rav1, the region that is predicted to be rich in β-sheet.

Interactions of Rav1 with V_o Subunit Vph1—We previously determined that V-ATPase complexes containing the Vph1 isoform of the V_o a subunit require RAVE for assembly and function (13). We also found that Vph1NT bound to full-length Rav1 in the two-hybrid assay and determined that purified Vph1NT could bind to a fragment of Rav1 containing amino acids 840–1125 (13). To further explore binding of Vph1NT on Rav1, we again examined interactions with fragments and deletions in *RAV1* by two-hybrid assay. We expressed a small segment (Rav1 679–840) extending from the end of the N-terminal domain through the beginning of the highly conserved C-terminal domain. This region displayed a strong two-hybrid interaction with Vph1NT, but not with V_1 subunits or Rav2 (Fig. 2). Vph1NT also showed a strong two-hybrid interaction with the fragment corresponding to the N-terminal 240 amino acids of Rav1. Interestingly, Vph1NT did not interact with any of the Rav1 deletion constructs, except for a weak interaction with the Δ840 to stop construct, even though a number of these constructs contain the 1–240 fragment, 679–840 fragment, or both of these fragments. Even the two-hybrid construct lacking only the functionally dispensable last 87 amino acids failed to interact with Vph1NT, although it interacted with all of the other partners tested. These results suggest that the Rav1(1–240) and (679–840) fragments may contain binding sites for the Vph1NT but that these fragments either assume a different structure in the larger Rav1 constructs or contain binding sites that are masked in the larger constructs.

In light of the strong two-hybrid interaction between the Rav1(679–840) fragment and Vph1NT, we expressed a fragment of Rav1 containing amino acids 679–898 as an N-terminal MBP and C-terminal His$_6$-tagged construct in *E. coli* and then purified the Rav1(679–898)-His$_6$ protein and tested for binding of Vph1NT(1–372). As shown in Fig. 4, Vph1NT(1–372) binds to this fragment, consistent with a direct binding site in this region of Rav1. There was no binding of Vph1NT(1–372) to the TALON resin in the absence of the Rav1 fragment.

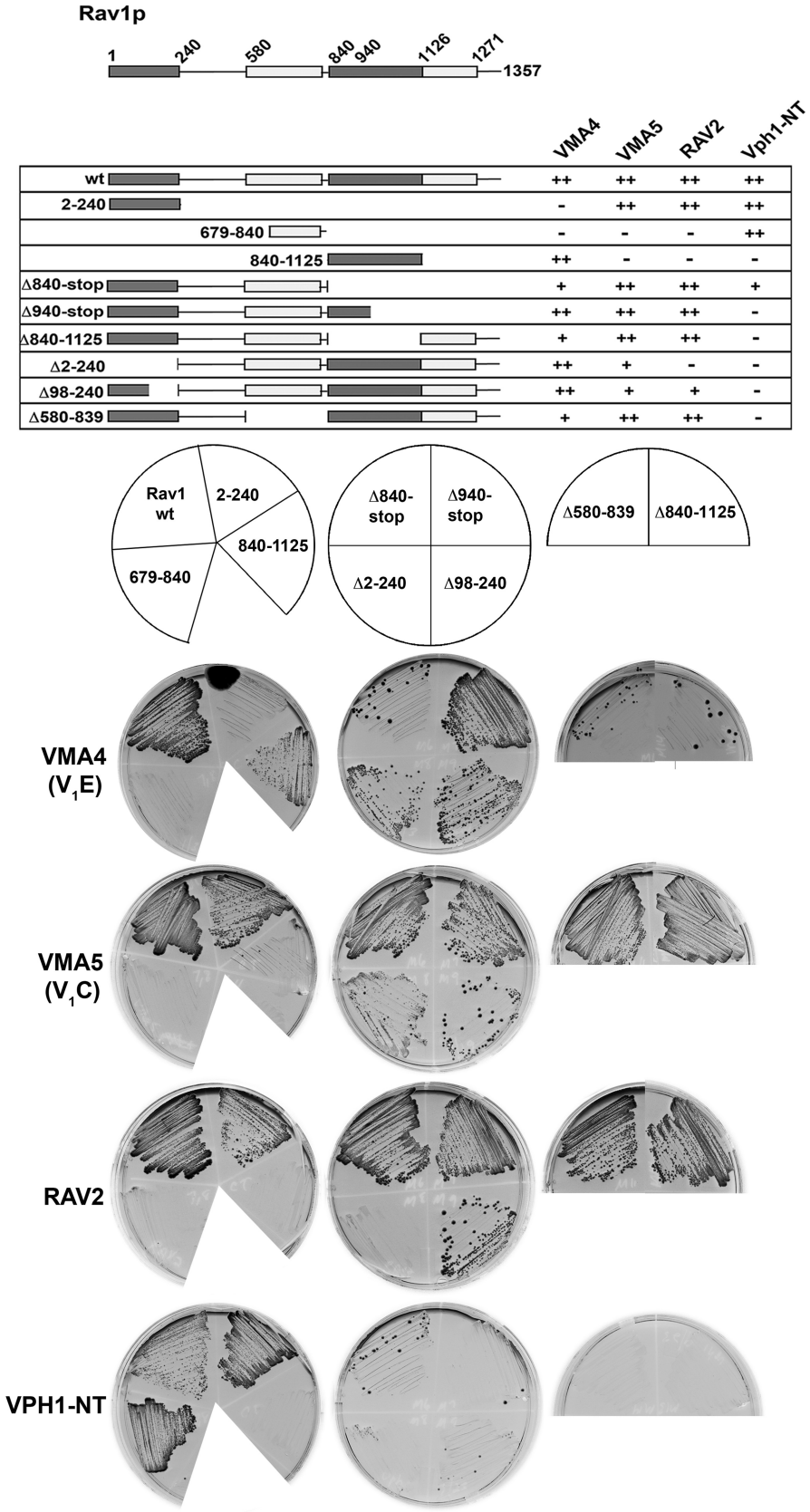

FIGURE 2. **Regions of Rav1 required for binding to Rav1 binding partners.** Rav1 fragments and deletions were cloned into the pAS two-hybrid plasmid as described in "Experimental Procedures." All pAS plasmids containing Rav1 fragments or deletions were transformed into the *MAT***a** PJ694A two-hybrid reporter strain. Each of these strains was crossed separately to each *MAT*α PJ694α strain containing either pACT-VMA4, pACT-VMA5, pACT-RAV2, or pACT-VPH1-NT, and diploids containing both plasmids were selected on SC medium lacking leucine and tryptophan. Diploids were then tested for expression of the two-hybrid reporter genes by plating on plates lacking adenine and histidine. The results shown are representative of at least three biological replicates.

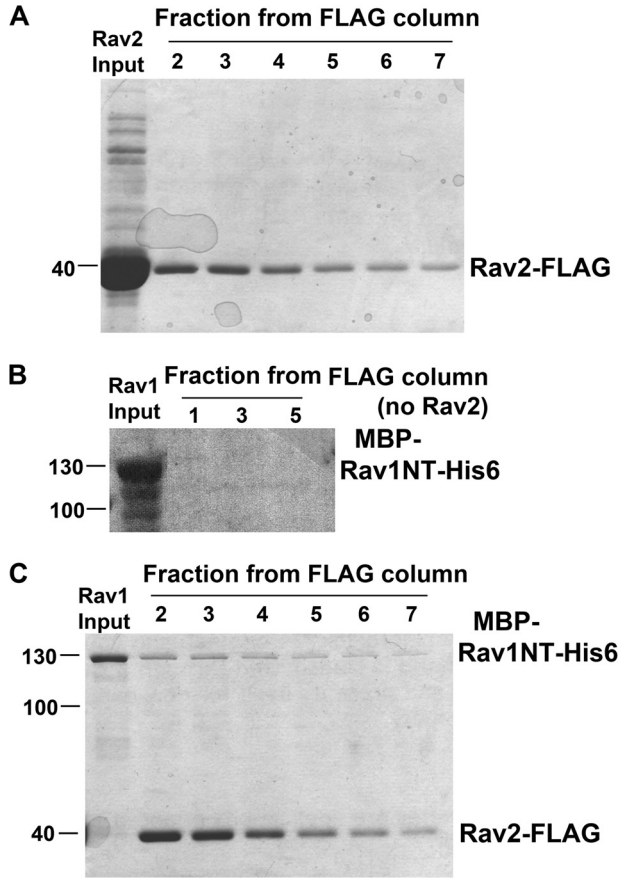

FIGURE 3. **Rav2 binds to the N-terminal domain of Rav1.** *A*, Rav2 was expressed as an MBP-Rav2-FLAG construct in *E. coli* and first purified via the MBP tag on an amylose affinity column. Rav2-FLAG was then cleaved from MBP by treatment with Prescission protease (Rav2 input) and further purified by anti-FLAG affinity chromatography. A Coomassie-stained gel of the input and fractions eluted from the anti-FLAG column after addition of FLAG peptide is shown. *B*, Rav1NT does not bind nonspecifically to anti-FLAG resin. Rav1(2–729) was expressed in *E. coli* as an MBP-Rav1NT-His_6 fusion. Protein fractions eluted from the amylose column after washing were combined and are shown as Rav1 input. The combined fractions (without cleavage of MBP) were added to the anti-FLAG M2 column and eluted with FLAG peptide after washing as in *A*. *C*, MBP-Rav1NT-His_6 was further purified on a TALON column. Protein-containing fractions eluted with imidazole from the TALON column were combined (Rav1 input) and added to an anti-FLAG column to which Rav2-FLAG had already been bound and washed but not eluted. After further washing, MBP-Rav1NT-His_6 co-elutes with Rav2-FLAG upon addition of FLAG peptide. Positions of molecular mass markers included on the gel are shown at *left*.

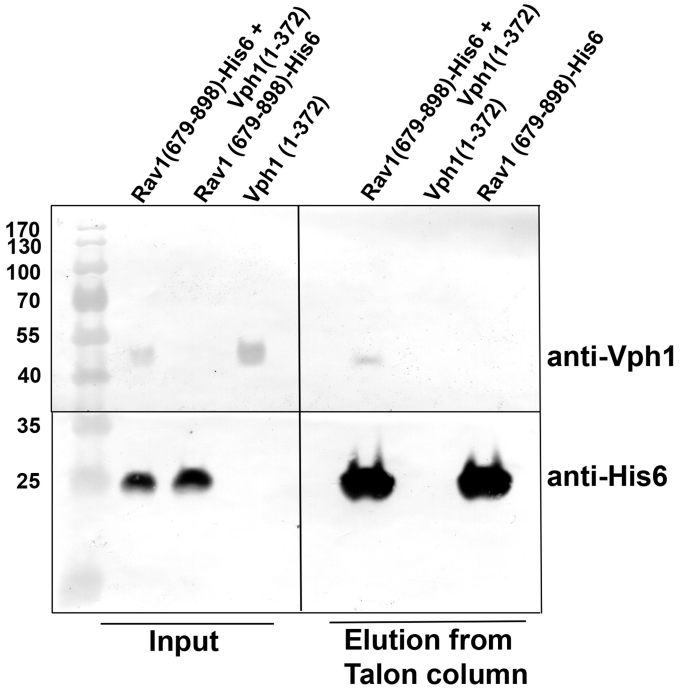

FIGURE 4. **Interaction of Rav1(679–898) with V_o subunit Vph1.** MBP-Rav1(679–898)-His_6 and MBP-Vph1(1–372) were expressed and purified, and the MBP was removed by cleavage as described under "Experimental Procedures." After cleavage, the two proteins were incubated individually and in combination (input) with 0.5 ml of TALON resin, which binds the His_6 tag. The resin was washed, and bound protein was eluted with imidazole as described under "Experimental Procedures." Parallel elution fractions from each condition were combined and precipitated. Equal proportions of the eluant were separated by SDS-PAGE and transferred to nitrocellulose. A single blot was cut at the *horizontal line* and probed with anti-Vph1 (*top*) or anti-His_6 (*bottom*) antibody. The sizes of molecular mass standards are shown at *left*.

Evidence for Binding Sites for the V_1 C Subunit on both Rav1 and Rav2—The V_1C subunit is likely to be a critical player in reassembly of the V-ATPase. This subunit binds at the interface of V_1 and V_o and is released from both sectors upon glucose deprivation (6, 14, 17). The two-hybrid experiments in Fig. 2 did not reveal a clear binding domain for subunit C. Previous two-hybrid experiments indicated interactions of subunit C with both intact Rav1 and Rav2. There was considerable overlap between regions of Rav1 that bound to Rav2 in the two-hybrid assay shown in Fig. 2 and those that showed interactions with subunit C. This is suggestive of bridging interactions in the two-hybrid assay and could indicate that V_1C is binding to Rav1 only through Rav2. However, there are also fragments, such as the Rav1Δ2–240 fragment, that exhibited a two-hybrid interaction with the C subunit but not to Rav2 (Fig. 2). To test whether there was direct binding between Rav1 and subunit C, we tested for binding of expressed and purified V_1C to a previously described fusion of GST to Rav1(840–1125) expressed in *E. coli* (13). As shown in Fig. 5*A*, subunit C co-eluted from glutathione-Sepharose with GST-Rav1(840–1125), and the identity of subunit C was confirmed by immunoblotting. (No expressed subunit C bound to glutathione-Sepharose in the absence of GST-tagged Rav1.) These data support a direct interaction of subunit C with Rav1, even though the Rav(840–1125) two-hybrid construct did not show binding to subunit C in Fig. 2. We next tested whether there was a separate site for subunit C binding on Rav2 by testing for interactions of the proteins expressed and purified from *E. coli* (Fig. 5*B*). Although purified V_1C showed low level binding to anti-FLAG resin in the absence of Rav2-FLAG, there was much better binding in the presence of Rav2-FLAG, indicating a direct interaction. To confirm that the Rav2-V_1C subunit interaction also occurred in yeast cells, we replaced the endogenous copy of the *VMA5* gene with a FLAG-tagged version, in wild type and *rav1*Δ mutant cells containing a C-terminally tagged Rav2p (Rav2-myc_{13}). As shown in Fig. 5*C*, Rav2-myc_{13} was co-immunoprecipitated by FLAG-tagged V_1C from both wild type and *rav1*Δ cells but was not bound to the anti-FLAG resin in the absence of a FLAG tag on subunit C. These results indicate that Rav2 and Rav1 can each bind independently to V_1C. This might suggest two binding sites for subunit C in the RAVE complex, but in the absence of additional structural

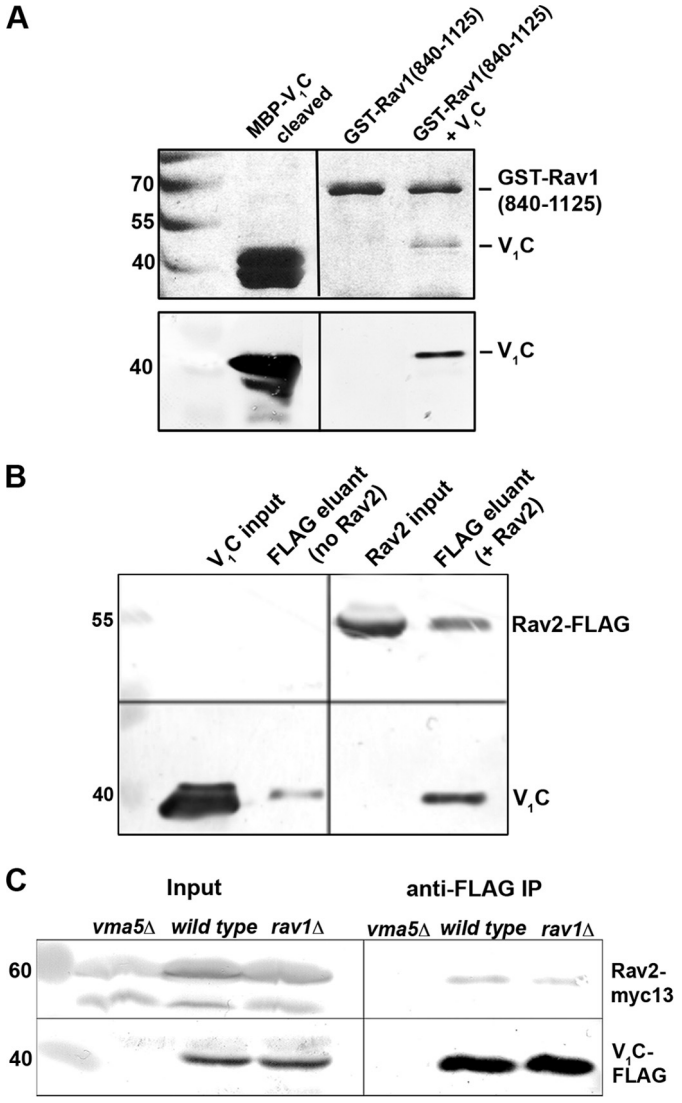

FIGURE 5. **V_1 subunit C binds to both Rav1 and Rav2.** *A*, the V_1C subunit was expressed as an MBP fusion protein (MBP-V_1C) and purified by amylose chromatography as described under "Experimental Procedures," and then the MBP tag was removed with Prescission protease (MBP-V_1C cleaved). GST-Rav1(840–1125) was expressed and purified on glutathione-Sepharose as described (13). The GST-Rav1(840–1125) fragment was eluted directly from one column, and V_1C was added to a second column, incubated with the GST-bound protein, and then eluted with glutathione. *Top gel*, Coomassie-stained gel; *bottom gel*, immunoblot with anti-C subunit antibody. Nonadjacent lanes from the same gels are shown; the *vertical line* represents the deleted lanes. *B*, V_1C input was prepared as in *A* and applied directly either to an anti-FLAG M2 column followed by washing and elution with FLAG peptide (no Rav2) or to an anti-FLAG column to which Rav2-FLAG had been bound as in Fig. 3, followed by washing and elution (FLAG eluant +Rav2). The *top panel* is an anti-FLAG immunoblot, and the *bottom panel* is an anti-V_1C subunit immunoblot. Nonadjacent lanes from the same gels are shown in both panels; the *vertical line* represents the deleted lanes. *C*, A FLAG-tagged version of the subunit C gene (*VMA5*) was integrated at the *VMA5* locus in wild type yeast cells and a *rav1*Δ mutant. Both strains also contained an integrated myc_{13}-tagged Rav2. Immunoblots of Rav2-myc_{13} from total cell yeast lysates (*Input*) and anti-FLAG immunoprecipitations (*anti-FLAG IP*) are shown in the *top panel*. Immunoblots of the same samples with anti-FLAG are shown on the *bottom*. The *vma5*Δ samples lack any V_1C and serve as a negative control. Nonadjacent lanes of the same gel are shown in *A* and *B*.

information, it is not possible to exclude the possibility of a single site for C subunit binding with interfaces provided by both Rav1 and Rav2.

RAVE Shows Glucose-dependent Interactions with the Vacuolar Membrane—RAVE functions in promoting glucose-dependent assembly of V_1 and V_o sectors of the V-ATPase. In the absence of glucose, the RAVE complex can be isolated from soluble, cytosolic fractions in combination with V_1 subunits. However, Rav1 also binds to V_o subunit Vph1, suggesting that it may localize to membranes under certain conditions. Previous efforts to localize RAVE have given conflicting information (9, 37). We introduced a C-terminal GFP tag to both *RAV1* and *RAV2* and confirmed that the tagged strains were functional, because neither exhibited a *rav1*Δ growth phenotype. We then assessed the localization of Rav1-GFP and Rav2-GFP constructs in the presence of glucose and during glucose deprivation and readdition. As shown in Fig. 6, Rav2-GFP and Rav1-GFP both distribute between the vacuolar membrane, the cytosol, and several cytosolic puncta in cells maintained in glucose. (Yeast vacuoles appear as indentations under differential interference contrast microscopy.) Notably, under these conditions, V_1 and V_o sectors are predominantly assembled (6). We next asked whether localization would change when cells are deprived of glucose and disassembly of the V-ATPase occurs. Rav1-GFP and Rav2-GFP are largely released into the cytosol after 15 min of glucose deprivation. However, within 15 min after glucose readdition, both GFP-tagged RAVE subunits rebind to the vacuolar membrane. Previous results have established that RAVE is a stable complex both in the presence and absence of glucose (10, 11), so the very similar movements of Rav1-GFP and Rav2-GFP in response to glucose deprivation were expected. Importantly, these results are entirely consistent with the role of RAVE in V_1-V_o assembly. V_1 sectors and subunit C lose tight association with Vph1-containing V_o sectors at the vacuolar membrane upon glucose deprivation and reassemble with V_o upon glucose readdition (6, 9, 17).

Glucose-dependent Interaction of RAVE with the Membrane Does Not Require the C Subunit—Given the key role of the V_1C subunit in V_1-V_o assembly, we hypothesized that the V_1 C subunit might be required for membrane localization of the RAVE complex. In a *vma5*Δ mutant that lacks V_1C, V-ATPase activity in the vacuoles is lost (30). V_1 and the V_o sectors can partially assemble, but the V_1-V_o interaction appears to be destabilized. In support of this, V_1 sectors are lost during vacuole isolation from *vma5*Δ cells (30), but V_1 is distributed between the vacuole and cytosol as visualized in *vma5*Δ cells by immunofluorescence microscopy (18). Fig. 7 demonstrates that Rav2-GFP showed a wild type distribution, including staining at the vacuolar membrane and cytosolic puncta in a *vma5*Δ mutant maintained in glucose. We next asked whether Rav2-GFP localization would respond to glucose deprivation. As shown in Fig. 7, Rav2-GFP was released from the membrane by glucose deprivation and recruited back to the membrane by glucose readdition. Thus V_1C is not required for glucose-dependent recruitment and release of RAVE from the membrane.

Discussion

RAVE/V-ATPase Binding Sites Suggest a Role for RAVE in Orienting V_1 Peripheral Stalks, V_1C and V_o Vph1NT in V-ATPase Assembly—Consistent with RAVE functioning as a V-ATPase assembly factor, RAVE binds to all three compo-

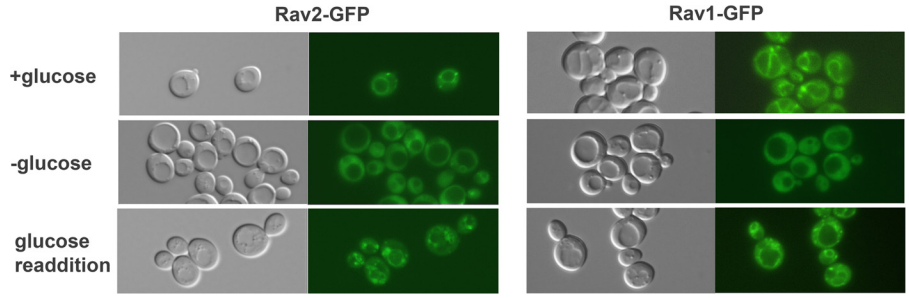

FIGURE 6. **RAVE shows glucose-dependent interactions with the vacuolar membrane.** Log phase cells from strains containing an integrated C-terminally tagged Rav1-GFP or Rav2-GFP were visualized directly by fluorescence microscopy as described under "Experimental Procedures." Cells were first visualized in growth media containing glucose. Cells were then visualized after pelleting, washing, and resuspending in media lacking glucose. Glucose-deprived cells were again pelleted and resuspended in media containing glucose. The images shown are representative of those seen in three independent experiments.

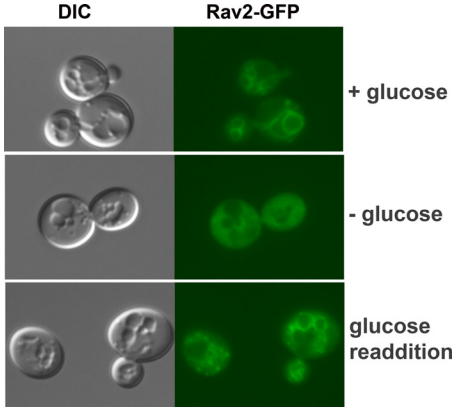

FIGURE 7. **Glucose-dependent interaction of RAVE with the vacuolar membrane does not require the V_1 C subunit.** A *vma5*Δ mutation was introduced into the Rav2-GFP strain, and the cells were treated and visualized as in Fig. 6. The images shown are representative of those seen in three independent experiments. *DIC*, differential interference contrast.

nents of the V-ATPase that are dissociated during glucose deprivation: the V_1 subcomplex via the E and G subunits (10), the V_1 C subunit (18), and V_o subunit Vph1 (13). The overall affinity of the V_1 sector for the V_o sector appears to be derived from distinct interactions of three V_1 EG-containing peripheral stalks at the V_1-V_o interface (14). We propose that RAVE is important in establishing key interactions with these stalks at the V_1-V_o interface. The V_1C subunit interacts in a defined orientation with two of the three EG peripheral stalks at the V_1-V_o interface of the assembled complex (38). V_1C is thus positioned to play a critical role in reversible disassembly, and consistent with this role, post-translational modifications of V_1C, as well as cytoskeletal interactions, have been implicated in reversible disassembly in other systems (17, 39). The third EG peripheral stalk interacts with the V_1H subunit and maintains this interaction in both the assembled and disassembled complex (4, 31, 38). We have found no evidence of RAVE interactions with V_1H (10), suggesting that this stalk is not directly affected by RAVE intervention in assembly.

We propose that the RAVE complex acts as an escort to bring the V_1 subcomplex, V_1 subunit C, and V_o together. Rav1 is the largest subunit and the central component of the RAVE complex. Rav2 and Skp1 bind to Rav1 but not to each other (9). Brace *et al.* (37) identified a *skp1* mutation that separated the essential Skp1 function in ubiquitin ligases from its role in RAVE and used this mutation to show that Skp1 is not required for V-ATPase assembly but may assist in release of RAVE from the membrane. This implicates Rav1 and Rav2 in promotion of V-ATPase assembly. Rav1 is responsible for the interaction between RAVE and V_1 (10) and also appears to contain the V_o interaction site (13). As shown in Fig. 5 and described below, subunit C binds to both Rav1 and Rav2. Rav1 is thus positioned to bind to both V_1 and V_o during assembly and to act with Rav2 to orient subunit C at the V_1-V_o interface.

To go beyond secondary structure prediction and Rav1 and/or rabconnectin sequence comparisons for interpreting the binding interactions we mapped across Rav1, we asked whether larger conserved structural elements could be identified in Rav1 using a structural bioinformatics approach. Submission of the entire *RAV1* sequence to the Phyre 2 server (41) gave a strong predicted model (100% estimated confidence that a remote homology has been identified and modeled well) for amino acids 55–669 of Rav1, based on alignment with *Caenorhabditis elegans* Aip1 (model c1nr0a). Although the model is based on remote homology, this level of confidence strongly suggests that the homology is real, and the overall fold is likely to be valid (41). The model consists of a double seven-bladed β-propeller structure (Fig. 8*A*). Such β-propeller structures are comprised of a series of WD or WD-like repeats, each containing four antiparallel β-sheets. Motif-based predictions had identified up to eight rather weakly conserved WD and WD-like repeats in Rav1 (25), but none had predicted 14 WD repeats. Interestingly, motif predictions had identified 7–10 WD repeats in Aip1 prior to structure determination (42), indicating that these motif predictions can be incomplete. In fact, not only the highest scoring structure for Rav1 but also the next five structures all predict double β-propellers covering a similar region of Rav1. Because the hits from submission of the entire *RAV1* sequence were overwhelmingly directed toward the N-terminal β-sheet-rich region, we submitted the sequence for amino acids 760–1270, which contains the α-helical region, separately. The highest confidence model (97.5% confidence) aligned a small portion of this sequence, amino acids 967–1081 of *RAV1*, with a helical region of the β′ subunit of the COP I coatomer (model c3mkqA). This model is also shown in Fig. 8*A*. Interestingly, this region of the β′ subunit of COP I forms an α solenoid structure and is adjacent to a double β-propeller structure at the N terminus of this protein (43).

In Fig. 8*A*, we map binding sites for Rav1 binding partners to regions within the N- and C-terminal halves of Rav1. The Rav1

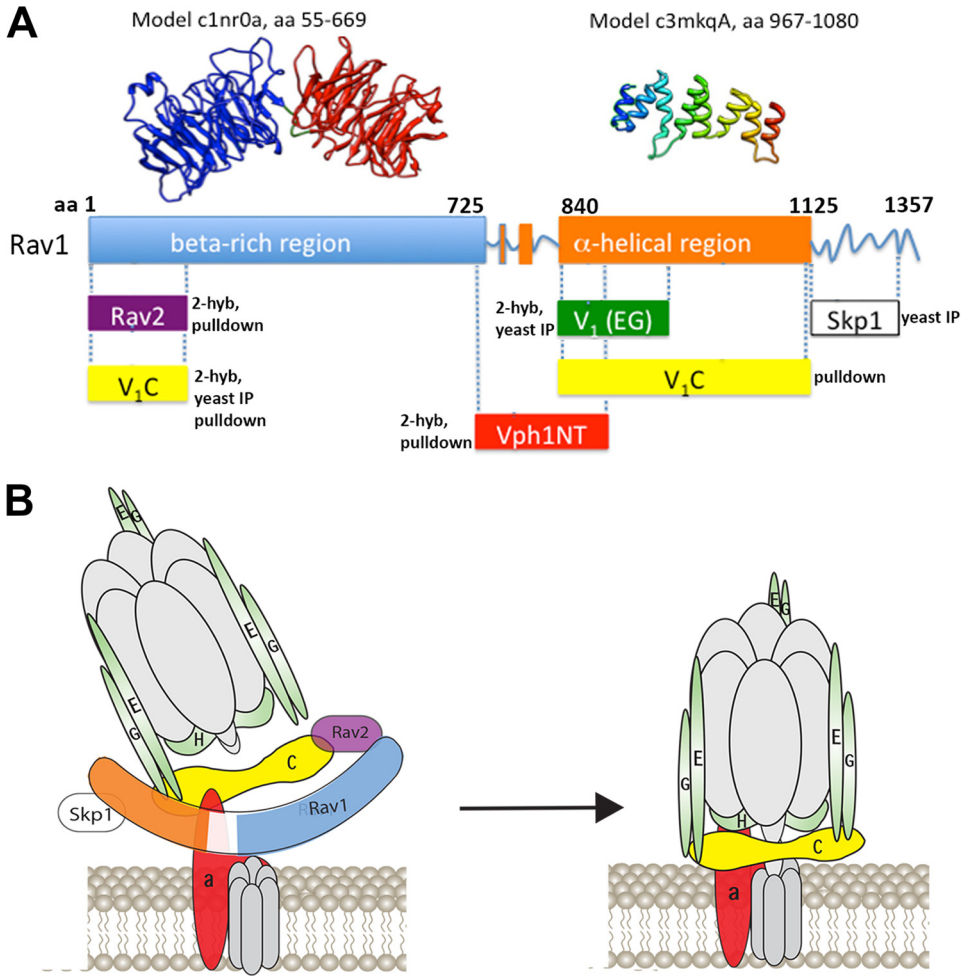

FIGURE 8. **Summary of modeling and interactions of yeast Rav1, the central subunit of the RAVE complex.** *A*, submission of the entire Rav1 sequence to the Phyre2 server generated a model for amino acids 55–669 based on *C. elegans* Aip1 (c1nr0a). Submission of Rav1 amino acids 760–1270 only resulted in a high confidence model for amino acids 967–1080 of the highly conserved region of Rav1, based on the COPI β′ subunit (c3mkqA). These models are shown above regions of interaction determined here for different Rav1 binding partners. The lengths of the *bars* indicate the delimited region of interaction, not the size of the interaction partner. The types of experiment supporting the interaction are also indicated. Secondary structure domains in Rav1 correspond to those shown in Fig. 1. *B*, model depicting potential roles of Rav1 interactions (colored as in *A*) during reassembly of the V-ATPase.

C-terminal α-helical region contains the most conserved sequence among Rav1 homologues (amino acids 840–1125) (25). Immunoprecipitations from C-terminal deletions of *RAV1* suggest a requirement for amino acids 840–940 for V_1 binding and for amino acids 1126–1271 for Skp1 binding (Fig. 1). Interestingly, two Rav1 mutants, Δ940-stop and Δ1126-stop were able to bind V_1 at wild type levels but had compromised binding to Skp1; these mutations were not able to rescue the *rav1*Δ phenotype. This result suggests that both V_1 and Skp1 binding in the C-terminal half of Rav1 are necessary for RAVE activity and that Skp1 plays an essential role in RAVE function despite evidence that it is not essential for assembly (37). Two-hybrid data (Fig. 2) support the interaction of the highly conserved Rav1(840–1125) region with V_1 subunit E and are consistent with the requirement for amino acids 840–890 suggested by immunoprecipitations in Fig. 1.

The N-terminal half of Rav1 supports the interaction with Rav2 (Figs. 2 and 3). The expressed Rav1(2–729) and Rav2 proteins proved to interact *in vitro* (Fig. 3). The second most conserved region of *RAV1* is the first 240 amino acids of the N-terminal domain. Further two-hybrid experiments using deletions of Rav1 in this region suggest that Rav2 requires the first 98 amino acids of Rav1 for binding. This Rav1(1–240) conserved region also interacted with V_1C and Vph1NT in a two-hybrid assay (Fig. 2). We have not yet confirmed these interactions *in vitro*, so it is possible that these two-hybrid interactions (particularly those between V_1C and Rav1(1–240)) could be indirect, possibly caused by bridging by Rav2.

Previous two-hybrid data indicated an interaction of subunit C with both Rav1 and Rav2 (18). In Fig. 5, we present the first evidence for direct binding of subunit C to both Rav1(840–1125) and Rav2. The possibility of two distinct binding sites is important because it suggests a role for RAVE in orienting subunit C, which must establish interactions to two different peripheral stalks, during assembly. As described above, the V_1 C subunit is localized to the interface of V_1 and V_o and likely to be a critical player in V-ATPase assembly. In EM reconstructions and cryo-EM structures, subunit C binds to two of the three peripheral EG peripheral stalks (38, 44–46). The crystal structure of subunit C shows three domains, a globular "head" (C_{head}), an elongated "neck," and another globular "foot" (C_{foot}) (47). Subsequent work with purified subunits showed

that C_{head} binds to EG with high affinity *in vitro* to form a stable EGC_{head} complex (15, 48). The lower affinity of C_{foot} for the EG heterodimer precludes the formation of a complex *in vitro*, but both C_{foot} and EG bind Vph1NT with low affinity, and it has been suggested that a high avidity quaternary complex forms, including C_{foot}, EG, and Vph1NT (14, 15). Data showing cross-linking between C_{foot} and the N-terminal region of Vph1 support this possibility (49).

We had previously demonstrated that a purified Rav1(840–1125) fragment could bind to Vph1NT (13). We provide evidence here that Rav1(679–840), which lies just upstream of the most conserved region and contains the junction between the N- and C-terminal halves of Rav1, interacts with Vph1NT in two-hybrid assay. This interaction is further supported by *in vitro* binding of purified Vph1NT to expressed Rav1(679–898)-His_6 (Fig. 4). Taken together, the arrangement of interaction sites for Vph1NT, V_1 (through the EG peripheral stalks) and V_1 subunit C on RAVE supports the proposition that RAVE could serve as a template for V_1 and V_o assembly by helping to bring the two V-ATPase subdomains into proximity and properly orienting subunit C to promote the assembly process. A possible model for RAVE intervention in assembly is shown in Fig. 8*B*.

RAVE Is Recruited to the Vacuolar Membrane in a Glucose-dependent Manner—Although the requirement for RAVE in V-ATPase reassembly had been known for some time, we present here the first evidence that the RAVE complex itself is reversibly recruited to the vacuolar membrane in the presence of glucose, conditions that promote V-ATPase reassembly. In Fig. 6, we show that RAVE is localized primarily to the vacuolar membrane with some staining in the cytosol and a few smaller puncta when cells are maintained in glucose. When cells are subsequently deprived of glucose, RAVE is released from the vacuolar membrane into the cytosol but is able to rebind to the membrane upon glucose readdition. This is entirely consistent with evidence for the assembly of V_1 and V_0 at the vacuolar membrane in the presence of glucose and the disassembly and release of V_1 and subunit C into the cytosol in the absence of glucose (6, 7, 40). It is more difficult to reconcile with recent data suggesting that GFP-tagged V_1 subunits other than subunit C remain in proximity to the membrane when cells are deprived of glucose (17). We previously found increased co-immunoprecipitation of RAVE subunits with V_1 in cytosolic fractions from glucose-deprived cells (10). This result supports release of V_1 sectors from the vacuolar membrane with glucose deprivation and implicates V_1 binding to RAVE as a mechanism for sequestering V_1 from V_o and/or priming V_1 for reassembly upon glucose readdition (10). However, if V_1 sectors lacking subunit C remain near the membrane during glucose deprivation and RAVE subunits are released almost completely from the vacuolar membrane, it is hard to envision how RAVE could act on V_1 to promote assembly. V_1 subunit C can bind to RAVE independently of V_1 (18), so it is possible that RAVE-subunit C complexes are released to the cytosol upon glucose deprivation and that RAVE sequesters subunit C and/or primes it for rebinding upon glucose readdition. These questions require further investigation.

Interestingly, RAVE is able to localize to the vacuolar membrane in the absence of the V_1 C subunit, and its localization responds to glucose deprivation and readdition similarly to wild type cells (Fig. 7). This is consistent with previous results indicating partial assembly of inactive and unstable V_1-V_o complexes at the vacuolar membrane in the absence of subunit C (18, 30). However, these results also have implications for the nature of glucose signaling to the V-ATPase and the RAVE complex. We previously showed that under conditions where V_1 was not able to assemble with V_o, the cytosolic V_1-RAVE interaction did not change with glucose deprivation, suggesting that this interaction is not intrinsically glucose-sensitive (10). As described above, work in other systems had implicated subunit C in reversible disassembly and suggested that it might be a direct recipient of glucose signals (39). However, glucose-responsive recruitment of RAVE to the vacuolar membrane in the absence of subunit C indicates that there must be glucose-dependent signals that do not depend on V_1C. These signals could be focused on the RAVE-V_o interaction, but further experiments will be necessary to identify the nature and location of this signal.

Author Contributions—A. M. S. designed, performed, and analyzed the experiments in Figs. 2 and 3 and contributed to Fig. 7 and to writing the paper. M. T. designed, performed, and analyzed the experiments in Figs. 6–8. N. D. N. and T. T. D. designed, performed, and analyzed the experiments in Figs. 4 and 5. P. M. K. conceived and coordinated the study and wrote the paper. All authors reviewed the results and approved the final version of the manuscript.

Acknowledgments—We thank Rebecca Oot and Stephan Wilkens for the MBP-Vph1(1–372) construct.

References

1. Kane, P. M. (2006) The where, when, and how of organelle acidification by the yeast vacuolar H^+-ATPase. *Microbiol. Mol. Biol. Rev.* **70,** 177–191
2. Forgac, M. (2007) Vacuolar ATPases: rotary proton pumps in physiology and pathophysiology. *Nat. Rev. Mol. Cell Biol.* **8,** 917–929
3. Gräf, R., Harvey, W. R., and Wieczorek, H. (1996) Purification and properties of a cytosolic V1-ATPase. *J. Biol. Chem.* **271,** 20908–20913
4. Parra, K. J., Keenan, K. L., and Kane, P. M. (2000) The H subunit (Vma13p) of the yeast V-ATPase inhibits the ATPase activity of cytosolic V1 complexes. *J. Biol. Chem.* **275,** 21761–21767
5. Zhang, J., Myers, M., and Forgac, M. (1992) Characterization of the V_0 domain of the coated vesicle (H^+)-ATPase. *J. Biol. Chem.* **267,** 9773–9778
6. Kane, P. M. (1995) Disassembly and reassembly of the yeast vacuolar H^+-ATPase *in vivo*. *J. Biol. Chem.* **270,** 17025–17032
7. Sumner, J. P., Dow, J. A., Earley, F. G., Klein, U., Jäger, D., and Wieczorek, H. (1995) Regulation of plasma membrane V-ATPase activity by dissociation of peripheral subunits. *J. Biol. Chem.* **270,** 5649–5653
8. Kane, P. M. (2012) Targeting reversible disassembly as a mechanism of controlling V-ATPase activity. *Curr. Protein Pept. Sci.* **13,** 117–123
9. Seol, J. H., Shevchenko, A., and Deshaies, R. J. (2001) Skp1 forms multiple protein complexes, including RAVE, a regulator of V-ATPase assembly. *Nat. Cell Biol.* **3,** 384–391
10. Smardon, A. M., Tarsio, M., and Kane, P. M. (2002) The RAVE complex is essential for stable assembly of the yeast V-ATPase. *J. Biol. Chem.* **277,** 13831–13839
11. Seol, J. H., Feldman, R. M., Zachariae, W., Shevchenko, A., Correll, C. C., Lyapina, S., Chi, Y., Galova, M., Claypool, J., Sandmeyer, S., Nasmyth, K., and Deshaies, R. J. (1999) Cdc53/cullin and the essential Hrt1 RING-H2 subunit of SCF define a ubiquitin ligase module that activates the E2 en-

zyme Cdc34. *Genes Dev.* **13,** 1614–1626
12. Bai, C., Sen, P., Hofmann, K., Ma, L., Goebl, M., Harper, J. W., and Elledge, S. J. (1996) SKP1 connects cell cycle regulators to the ubiquitin proteolysis machinery through a novel motif, the F-box. *Cell* **86,** 263–274
13. Smardon, A. M., Diab, H. I., Tarsio, M., Diakov, T. T., Nasab, N. D., West, R. W., and Kane, P. M. (2014) The RAVE complex is an isoform-specific V-ATPase assembly factor in yeast. *Mol. Biol. Cell* **25,** 356–367
14. Oot, R. A., and Wilkens, S. (2012) Subunit interactions at the V_1-V_0 interface in yeast vacuolar ATPase. *J. Biol. Chem.* **287,** 13396–13406
15. Oot, R. A., and Wilkens, S. (2010) Domain characterization and interaction of the yeast vacuolar ATPase subunit C with the peripheral stator stalk subunits E and G. *J. Biol. Chem.* **285,** 24654–24664
16. Zhao, J., Benlekbir, S., and Rubinstein, J. L. (2015) Electron cryomicroscopy observation of rotational states in a eukaryotic V-ATPase. *Nature* **521,** 241–245
17. Tabke, K., Albertmelcher, A., Vitavska, O., Huss, M., Schmitz, H. P., and Wieczorek, H. (2014) Reversible disassembly of the yeast V-ATPase revisited under in vivo conditions. *Biochem. J.* **462,** 185–197
18. Smardon, A. M., and Kane, P. M. (2007) RAVE is essential for the efficient assembly of the C subunit with the vacuolar H^+-ATPase. *J. Biol. Chem.* **282,** 26185–26194
19. Sakisaka, T., and Takai, Y. (2005) Purification and properties of rabconnectin-3. *Methods Enzymol.* **403,** 401–407
20. Sethi, N., Yan, Y., Quek, D., Schupbach, T., and Kang, Y. (2010) Rabconnectin-3 is a functional regulator of mammalian notch signaling. *J. Biol. Chem.* **285,** 34757–34764
21. Yan, Y., Denef, N., and Schüpbach, T. (2009) The vacuolar proton pump, V-ATPase, is required for notch signaling and endosomal trafficking in *Drosophila*. *Dev. Cell* **17,** 387–402
22. Einhorn, Z., Trapani, J. G., Liu, Q., and Nicolson, T. (2012) Rabconnectin3α promotes stable activity of the H^+ pump on synaptic vesicles in hair cells. *J. Neurosci.* **32,** 11144–11156
23. Li, K. W., Chen, N., Klemmer, P., Koopmans, F., Karupothula, R., and Smit, A. B. (2012) Identifying true protein complex constituents in interaction proteomics: the example of the DMXL2 protein complex. *Proteomics* **12,** 2428–2432
24. Marchler-Bauer, A., Derbyshire, M. K., Gonzales, N. R., Lu, S., Chitsaz, F., Geer, L. Y., Geer, R. C., He, J., Gwadz, M., Hurwitz, D. I., Lanczycki, C. J., Lu, F., Marchler, G. H., Song, J. S., Thanki, N., Wang, Z., Yamashita, R. A., Zhang, D., Zheng, C., and Bryant, S. H. (2015) CDD: NCBI's conserved domain database. *Nucleic Acids Res.* **43,** D222–D226
25. Kane, P. M., and Smardon, A. M. (2003) Assembly and regulation of the yeast vacuolar H+-ATPase. *J. Bioenerg. Biomembr.* **35,** 313–321
26. Longtine, M. S., McKenzie, A., 3rd, Demarini, D. J., Shah, N. G., Wach, A., Brachat, A., Philippsen, P., and Pringle, J. R. (1998) Additional modules for versatile and economical PCR-based gene deletion and modification in *Saccharomyces cerevisiae*. *Yeast* **14,** 953–961
27. Wach, A. (1996) PCR-synthesis of marker cassettes with long flanking homology regions for gene disruptions in *S. cerevisiae*. *Yeast* **12,** 259–265
28. Gietz, D., St Jean, A., Woods, R. A., and Schiestl, R. H. (1992) Improved method for high efficiency transformation of intact yeast cells. *Nucleic Acids Res.* **20,** 1425
29. Wach, A., Brachat, A., Alberti-Segui, C., Rebischung, C., and Philippsen, P. (1997) Heterologous HIS3 marker and GFP reporter modules for PCR-targeting in *Saccharomyces cerevisiae*. *Yeast* **13,** 1065–1075
30. Ho, M. N., Hill, K. J., Lindorfer, M. A., and Stevens, T. H. (1993) Isolation of vacuolar membrane H^+-ATPase-deficient yeast mutants; the VMA5 and VMA4 genes are essential for assembly and activity of the vacuolar H^+-ATPase. *J. Biol. Chem.* **268,** 221–227
31. Diab, H., Ohira, M., Liu, M., Cobb, E., and Kane, P. M. (2009) Subunit interactions and requirements for inhibition of the yeast V1-ATPase. *J. Biol. Chem.* **284,** 13316–13325
32. Lowry, O., H., Rosebrough, N. J., Farr, A., L., and Randall, R., J. (1951) Protein measurement with the Folin phenol reagent. *J. Biol. Chem.* **193,** 265–275
33. Kane, P. M., Kuehn, M. C., Howald-Stevenson, I., and Stevens, T. H. (1992) Assembly and targeting of peripheral and integral membrane subunits of the yeast vacuolar H^+-ATPase. *J. Biol. Chem.* **267,** 447–454
34. Bai, C., and Elledge, S. J. (1997) Gene identification using the yeast two-hybrid system. *Methods Enzymol.* **283,** 141–156
35. James, P., Halladay, J., and Craig, E. A. (1996) Genomic libraries and a host strain designed for highly efficient two-hybrid selection in yeast. *Genetics* **144,** 1425–1436
36. Jones, D. T. (1999) Protein secondary structure prediction based on position-specific scoring matrices. *J. Mol. Biol.* **292,** 195–202
37. Brace, E. J., Parkinson, L. P., and Fuller, R. S. (2006) Skp1p regulates Soi3p/Rav1p association with endosomal membranes but is not required for vacuolar ATPase assembly. *Eukaryot. Cell* **5,** 2104–2113
38. Benlekbir, S., Bueler, S. A., and Rubinstein, J. L. (2012) Structure of the vacuolar-type ATPase from *Saccharomyces cerevisiae* at 11-A resolution. *Nat. Struct. Mol. Biol.* **19,** 1356–1362
39. Voss, M., Vitavska, O., Walz, B., Wieczorek, H., and Baumann, O. (2007) Stimulus-induced phosphorylation of vacuolar H^+-ATPase by protein kinase A. *J. Biol. Chem.* **282,** 33735–33742
40. Dechant, R., Binda, M., Lee, S. S., Pelet, S., Winderickx, J., and Peter, M. (2010) Cytosolic pH is a second messenger for glucose and regulates the PKA pathway through V-ATPase. *EMBO J.* **29,** 2515–2526
41. Kelley, L. A., Mezulis, S., Yates, C. M., Wass, M. N., and Sternberg, M. J. (2015) The Phyre2 web portal for protein modeling, prediction and analysis. *Nat. Protoc.* **10,** 845–858
42. Voegtli, W. C., Madrona, A. Y., and Wilson, D. K. (2003) The structure of Aip1p, a WD repeat protein that regulates Cofilin-mediated actin depolymerization. *J. Biol. Chem.* **278,** 34373–34379
43. Lee, C., and Goldberg, J. (2010) Structure of coatomer cage proteins and the relationship among COPI, COPII, and clathrin vesicle coats. *Cell* **142,** 123–132
44. Diepholz, M., Börsch, M., and Böttcher, B. (2008) Structural organization of the V-ATPase and its implications for regulatory assembly and disassembly. *Biochem. Soc. Trans.* **36,** 1027–1031
45. Zhang, Z., Zheng, Y., Mazon, H., Milgrom, E., Kitagawa, N., Kish-Trier, E., Heck, A. J., Kane, P. M., and Wilkens, S. (2008) Structure of the yeast vacuolar ATPase. *J. Biol. Chem.* **283,** 35983–35995
46. Rawson, S., Phillips, C., Huss, M., Tiburcy, F., Wieczorek, H., Trinick, J., Harrison, M. A., and Muench, S. P. (2015) Structure of the Vacuolar H^+-ATPase rotary motor reveals new mechanistic insights. *Structure* **23,** 461–471
47. Drory, O., Frolow, F., and Nelson, N. (2004) Crystal structure of yeast V-ATPase subunit C reveals its stator function. *EMBO Rep.* **5,** 1148–1152
48. Oot, R. A., Huang, L. S., Berry, E. A., and Wilkens, S. (2012) Crystal structure of the yeast vacuolar ATPase heterotrimeric EGC(head) peripheral stalk complex. *Structure* **20,** 1881–1892
49. Inoue, T., and Forgac, M. (2005) Cysteine-mediated cross-linking indicates that subunit C of the V-ATPase is in close proximity to subunits E and G of the V1 domain and subunit a of the V0 domain. *J. Biol. Chem.* **280,** 27896–27903